

## Water Oxidation

## Efficient Water Oxidation Catalyzed by Mononuclear Ruthenium(II) Complexes Incorporating Schiff Base Ligands

Ting-Ting Li,<sup>[a]</sup> Yong Chen,<sup>[a]</sup> Fu-Min Li,<sup>[b]</sup> Wei-Liang Zhao,<sup>[b]</sup> Chuan-Jun Wang,<sup>[a]</sup> Xiao-Jun Lv,<sup>[a]</sup> Quan-Qing Xu,<sup>[b]</sup> and Wen-Fu Fu<sup>\*[a, b]</sup>

**Abstract:** Four new charge-neutral ruthenium(II) complexes containing dianionic Schiff base and isoquinoline or 4-picoline ligands were synthesized and characterized by NMR and ESI-MS spectroscopies, elemental analysis, and X-ray diffraction. The complexes exhibited excellent chemical water oxidation activity and high stability under acidic conditions (pH 1.0) using (NH<sub>4</sub>)<sub>2</sub>Ce(NO<sub>3</sub>)<sub>6</sub> as a sacrificial electron accept-

or. The high catalytic activities of these complexes for water oxidation were sustained for more than 10 h at low concentrations. High turnover numbers of up to 3200 were achieved. A water nucleophilic attack mechanism was proposed. A Ru<sup>V</sup>=O intermediate was detected during the catalytic cycle by high-resolution mass spectrometry.

## Introduction

Photochemical water splitting is a promising strategy to convert solar energy into chemical energy to meet rising global energy demands.<sup>[1–3]</sup> The photolysis of water, which involves a multielectron process coupled with a multiproton transfer, consists of two half reactions whereby protons are reduced to dihydrogen and water is oxidized to dioxygen. Because this transformation requires energy ( $E^0 = 1.23$  V versus the normal hydrogen electrode, NHE), water oxidation is considered to be the key step of the water-splitting process.<sup>[4]</sup> In nature, water oxidation occurs in the photosystem II (PSII) and the tetranuclear manganese cluster (CaMn<sub>4</sub>O<sub>x</sub>) serves as the oxygen-evolving complex.<sup>[5–8]</sup> The metal centers in the complex can be oxidized to higher oxidation states to promote the transformation of metal-aquo to metal-oxo intermediates prior to dioxygen production.<sup>[9]</sup> Based on the PSII, chemists have attempted to develop water oxidation catalysts (WOCs) for artificial photosynthesis processes. Mono-, di-, and polynuclear Ru,<sup>[10]</sup> Ir,<sup>[11]</sup> Mn,<sup>[12]</sup> Fe,<sup>[13]</sup> and Co<sup>[14]</sup> complexes that exhibit catalytic characteristics have been reported. These complexes are easily oxidized to higher oxidation states in the presence

of strong oxidizing agents under acidic conditions, and undergo successive and simultaneous loss of protons and electrons through proton-coupled electron-transfer (PCET) processes. Most of those studies have focused on Ru-based catalysts. The first molecular WOC, blue dimer *cis,cis*-[(bpy)<sub>2</sub>(H<sub>2</sub>O)RuORu(H<sub>2</sub>O)-(bpy)<sub>2</sub>]<sup>4+</sup> (bpy = 2,2'-bipyridine), was pioneered by Meyer et al. in the early 1980s.<sup>[15]</sup> In 2005, Zong and Thummel reported a well-defined mononuclear ruthenium complex that can catalyze water oxidation processes in the presence of (NH<sub>4</sub>)<sub>2</sub>Ce(NO<sub>3</sub>)<sub>6</sub> (CAN).<sup>[16]</sup> More recently, Sun et al. employed 2,2'-bipyridine-6,6'-dicarboxylic acid (H<sub>2</sub>bda) as an anionic ligand to prepare mononuclear ruthenium complex [Ru(bda)(pic)<sub>2</sub>] (pic = 4-picoline), which displayed excellent catalytic activity towards water oxidation processes under both thermal and visible-light-driven conditions.<sup>[17]</sup> Furthermore, by replacing the axial ligand with isoquinoline (isoq), the prepared [Ru(bda)(isoq)<sub>2</sub>] was capable of chemically catalyzing water oxidation processes with a high turnover frequency of 303 s<sup>-1</sup>.<sup>[18]</sup> However, the catalytic lifespan of most Ru<sup>II</sup>-based WOCs is limited to the minute scale. The dissociation of axial ligands and oxidative decomposition of equatorial ligands have been considered as the major catalyst deactivation pathways.<sup>[15,19]</sup> Thus, the fabrication of WOCs with well-defined structures that have both a high turnover and a long catalytic lifespan remains a challenge.

To avoid decomposition of the organic ligands in molecular WOCs, some research groups have attempted to improve the durability of the catalytic system by immobilizing catalysts on the electrode surface, which dramatically suppressed the oxidative decomposition pathway.<sup>[20]</sup> Compared with heterogeneous systems, the longevity of WOCs in homogeneous systems can be extended by increasing the rigidity of the equatorial ligands. Compared to [Ru(bda)(pic)<sub>2</sub>] catalyst, Sun and co-workers discovered that [Ru(pda)(pic)<sub>2</sub>] complex bearing rigid ligand 1,10-phenanthroline-2,9-dicarboxylate (pda) exhibited im-

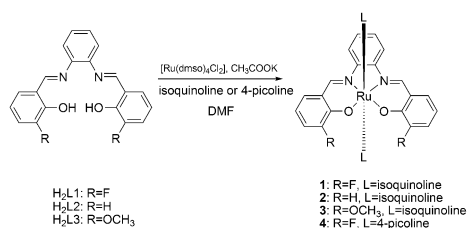
[a] T.-T. Li, Prof. Dr. Y. Chen, C.-J. Wang, Dr. X.-J. Lv, Prof. Dr. W.-F. Fu  
Key Laboratory of Photochemical Conversion and Optoelectronic Materials  
and HKU-CAS Joint Laboratory on New Materials, Technical Institute of  
Physics and Chemistry and University of Chinese Academy of Sciences  
Chinese Academy of Sciences  
Beijing 100190 (P. R. China)  
Fax: (+86) 10-6255-4670  
E-mail: fuwff@mail.ipc.ac.cn

[b] F.-M. Li, W.-L. Zhao, Dr. Q.-Q. Xu, Prof. Dr. W.-F. Fu  
College of Chemistry and Engineering  
Yunnan Normal University  
Kunming 650092 (P. R. China)

Supporting information for this article is available on the WWW under  
<http://dx.doi.org/10.1002/chem.201305011>.

proved catalytic stability and different catalytic water oxidation pathways.<sup>[21]</sup>

Based on coordination geometry, most WOCs feature nitrogen-heterocyclic ligands, such as polypyridyl and poly(pyrazolyl), but the ligands are generally more difficult to prepare and modify when compared with some other simple ligands. Considerable efforts have been devoted to developing new ligands for water oxidation. These ligands should meet the following requirements: 1) the synthetic process needs to be relatively easy and afford easy modulation of the structural, electronic, and electrochemical properties, and catalyst activity of the resulting complex; 2) high chemical and photochemical stability under strong oxidizing conditions; and 3) improved  $\pi$ -electron-donating capabilities, that is, negatively charged ligands, affording reduced metal complex oxidation potentials and catalytic overpotential. Schiff bases are suitable candidates that are easily synthesized from an aromatic amine and a carbonyl compound through nucleophilic addition. A variety of metal complexes featuring Schiff base ligands have been prepared and used extensively in thermal catalysis and synthetic reactions.<sup>[22]</sup> Herein, we report the synthesis of four mononuclear ruthenium complexes comprising dianionic Schiff base ligands (Scheme 1). The obtained complexes exhibit remarkable cata-



Scheme 1. Syntheses of complexes 1–4.

lytic activities towards chemical water oxidation in the presence of CAN as oxidant under acidic conditions. Despite their similar ligand structure, the complexes displayed markedly different catalytic activities. Notably, the complexes exhibited high stabilities, as indicated by the sustained catalytic activity over a period of > 10 h. To the best of our knowledge, this is the first report examining Ru<sup>II</sup> complexes incorporating a Schiff base ligand for catalytic water oxidation under acidic conditions.

## Results and Discussion

### Synthesis and characterization

The Schiff base ligands were synthesized by the procedure shown in the Supporting Information. The preparation of complex **1** was performed by heating a mixture of H<sub>2</sub>L1, [Ru(dmsO)<sub>4</sub>Cl<sub>2</sub>], and potassium acetate in *N,N*-dimethylformamide at 70 °C overnight under N<sub>2</sub> atmosphere, followed by addition of excess isoquinoline. The solvent was removed in vacuo and the resulting residue was purified by column chromatography

to afford dark red solid **1**. A similar procedure was adopted for the preparation of complexes **2–4**. <sup>1</sup>H NMR analysis revealed that the complexes featured a C<sub>2v</sub> symmetry (Figure S1 in the Supporting Information). Single crystals of **2** and **4** were grown by slow diffusion of diethyl ether into an acetonitrile solution; the corresponding molecular structures are shown in Figure 1.

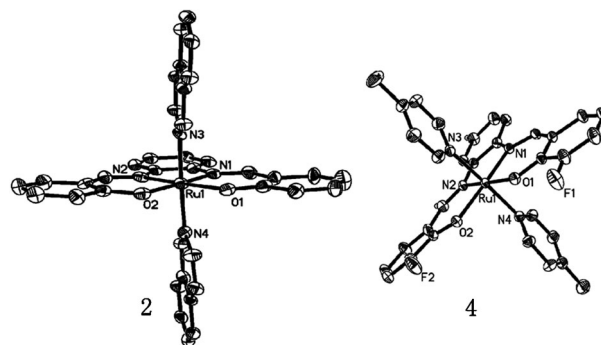


Figure 1. Molecular structures of **2** and **4** with thermal ellipsoids at 30% probability. Hydrogen atoms and solvents are omitted for clarity.

Detailed crystal data, and selected bond lengths and angles are listed in Table S1 in the Supporting Information and Table 1, respectively. The C<sub>2v</sub> symmetry around the Ru<sup>II</sup> center was further confirmed by X-ray analysis; the bond angles at the ruthenium atom vary from 82.3 to 95.1°.<sup>[23]</sup> The N atoms in the isoquinoline or 4-picoline ligands are bound to the metal in a nearly linear fashion for **2** and **4** with bond angles of 175.0 and 172.7°, respectively. The Ru–O1/O2 distances of 2.055(5)/2.066(5) Å in **2** are significantly shorter than those in [Ru(bda)(pic)]<sub>2</sub> and complex **4**.<sup>[17a]</sup> The Ru–N distances were within a range of 1.971–2.081 Å, which is similar to that of [Ru(bda)(pic)]<sub>2</sub>, and the axial Ru–N bond lengths of the complexes were slightly longer than the equatorial bonds. Intermolecular  $\pi$ – $\pi$  interactions of adjacent molecules along the *a* axis (Fig-

Table 1. Selected bond lengths [Å] and angles [°] for complexes **2** and **4**.

<b>2</b>		<b>4</b>	
Ru1–N1	1.971(6)	Ru1–N1	1.997(3)
Ru1–N2	1.993(6)	Ru1–N2	1.990(3)
Ru1–N3	2.081(5)	Ru1–N3	2.078(4)
Ru1–N4	2.071(5)	Ru1–N4	2.081(4)
Ru1–O1	2.055(5)	Ru1–O1	2.090(3)
Ru1–O2	2.066(5)	Ru1–O2	2.091(3)
N1–Ru1–N2	82.8(2)	N1–Ru1–N2	82.3(1)
N1–Ru1–N3	91.4(2)	N1–Ru1–N3	90.9(2)
N1–Ru1–N4	91.0(2)	N1–Ru1–N4	95.1(1)
N1–Ru1–O1	94.5(2)	N1–Ru1–O1	93.5(1)
N2–Ru1–N3	91.9(2)	N2–Ru1–N3	91.4(2)
N2–Ru1–N4	91.0(2)	N2–Ru1–N4	93.6(1)
N2–Ru1–O2	94.0(2)	N2–Ru1–O2	93.3(1)
N3–Ru1–O1	87.8(2)	N3–Ru1–O1	89.0(1)
N3–Ru1–O2	88.3(2)	N3–Ru1–O2	86.8(1)
N4–Ru1–O1	87.8(2)	N4–Ru1–O1	86.5(1)
N4–Ru1–O2	89.5(2)	N4–Ru1–O2	87.6(1)
O1–Ru1–O2	88.7(2)	O1–Ru1–O2	91.0(1)

ure S2 in the Supporting Information) are characterized by the short distance of about 3.2 Å between the planes of the two isoquinoline units.

### Absorption spectroscopy

The absorption spectra of **1–3** in acetonitrile are shown in Figure 2. Complex **1** displays strong bands in the near-UV region (200–300 nm), which correspond to intraligand  $\pi\text{-}\pi^*$

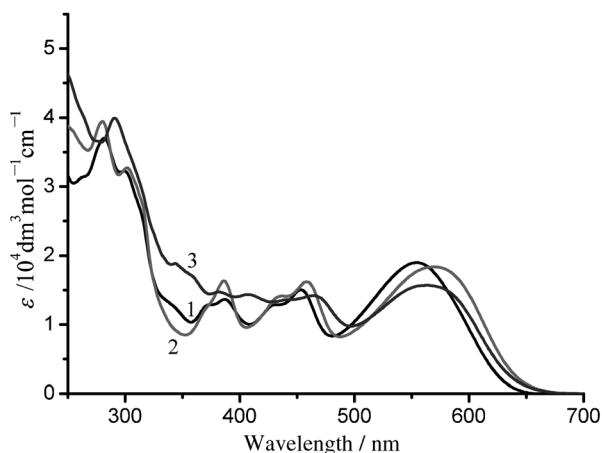


**Figure 2.** UV/Vis absorption spectra of complexes **1–3** ( $2.5 \times 10^{-5}$  M) in acetonitrile solution.

electron transitions. The characteristic long-wavelength absorptions in the visible region are assigned to metal-to-ligand charge-transfer (MLCT) transitions.<sup>[24,25]</sup> Although complexes **2** and **3** show similar absorption bands, complex **3** displays slightly weaker absorbance in the visible region when compared with those of **1** and **2**. The three complexes could be gradually oxidized by molecular oxygen under aerobic conditions in aqueous  $\text{CF}_3\text{SO}_3\text{H}$  solution (pH 1.0), which was accompanied by color changes from red to green. Spectral changes as a function of time for **2** in aqueous  $\text{CF}_3\text{SO}_3\text{H}$  solution under air atmosphere showed the reduced absorbance at around 560 nm that was assigned to the bleaching MLCT transitions, and the isosbestic points at 620, 582, and 625 nm were clearly observed in the time-resolved spectra of complexes **1**, **2**, and **3**, respectively, which indicated the existence of a new species (Figures S3–S5 in the Supporting Information). Based on high-resolution mass spectrometry (HRMS; found: 674.1214; calculated: 674.1261 for the complex **2**), this new species was tentatively ascribed to  $\text{Ru}^{\text{III}}$  complexes (Figure S6 in the Supporting Information). The  $^1\text{H}$  NMR spectrum of this green sample in  $\text{CDCl}_3$  featured broad signals, indicative of the formation of paramagnetic  $\text{Ru}^{\text{III}}$  species.<sup>[23]</sup> However, addition of an excess amount of ascorbic acid to the solution restored the absorption spectrum and original solution color (Figure S7 in the Supporting Information), thereby implying the reduction of  $\text{Ru}^{\text{III}}$  to  $\text{Ru}^{\text{II}}$ . After the isolated green solid was treated with ascorbic acid, its  $^1\text{H}$  NMR spectrum (Figure S1 in the Supporting Information) was identical with that of complex **2**. Addition of

1 equivalent of CAN to complex **2** in aqueous solution of pH 1.0 resulted in the bleaching MLCT band and increased absorbance around 430 nm. On adding a further 1 equivalent of CAN, the change in the higher-energy wavelength region only was observed (Figure S8 in the Supporting Information).

### Electrochemistry

The redox properties of complexes **1–3** were examined by cyclic voltammetry (CV) and differential pulse voltammetry (DPV) in both organic and mixed water solvents, and the electrochemical data are summarized in Table 2. The electrochemical behaviors of complexes **1–3** were first evaluated in dry acetonitrile, as shown in Figure 3. The complexes displayed markedly lower  $E_{1/2}(\text{Ru}^{\text{III/II}})$  values than those of WOCs containing neutral ligands.<sup>[26,27]</sup> The low potentials are most likely because of the improved  $\pi$ -electron-donating capabilities of the dianionic Schiff base ligands. Complex **1** with the electron-withdrawing (–F) group exhibits an  $E_{1/2}(\text{Ru}^{\text{III/II}})$  value of 0.28 V versus NHE, which is more positive than the corresponding potentials of **2** and **3**.

The DPV and CV curve of **3** in aqueous solution (pH 1.0) display three oxidation waves at 0.21, 0.61, and 1.23 V, corresponding to the oxidation potentials of  $E(\text{Ru}^{\text{III/II}})$ ,  $E(\text{Ru}^{\text{IV/III}})$ , and

**Table 2.** Oxidation potentials  $E_{\text{ox}}$  (V vs. NHE) of **1–3**.

Complex	$\text{Ru}^{\text{III/II}}$	$\text{Ru}^{\text{IV/III}}$	$\text{Ru}^{\text{IV/IV}}$
<b>1</b> <sup>[a]</sup>	0.31	–	–
<b>1</b> <sup>[b]</sup>	0.28	1.04	1.27
<b>2</b> <sup>[a]</sup>	0.22	0.65	1.25
<b>2</b> <sup>[b]</sup>	0.24	0.61	1.23
<b>3</b> <sup>[a]</sup>	0.19	–	–
<b>3</b> <sup>[b]</sup>	0.21	–	–

[a] Measured in acetonitrile containing 0.1 M  $(\text{Bu}_4\text{N})\text{PF}_6$ . [b] Measured in pH 1.0 solution (0.1 M  $\text{CF}_3\text{SO}_3\text{H}$ ) with 30% trifluoroethanol. The scan rate was  $100 \text{ mV s}^{-1}$ .  $[\text{Ru}(\text{bpy})_3]^{2+}$  was used as a reference with  $E_{1/2} = 1.26 \text{ V}$  vs. NHE.

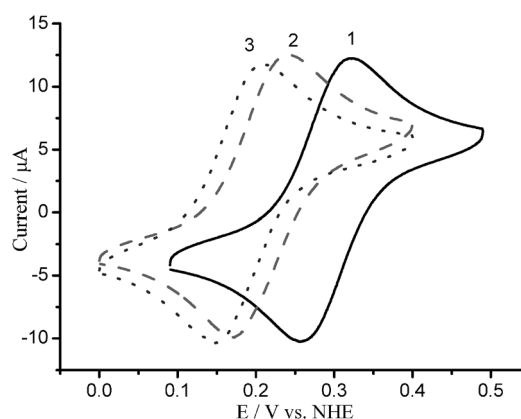


**Figure 3.** CV curves of complexes **1–3** (1.0 mM) in acetonitrile with  $(\text{Bu}_4\text{N})\text{PF}_6$  (0.1 M) as the supporting electrolyte, a glassy carbon disk as the working electrode, and  $\text{Ag}/\text{AgCl}$  as the reference electrode. Scan rate:  $100 \text{ mV s}^{-1}$ .

$E(\text{Ru}^{\text{V/IV}})$ , respectively (Figure 4). Complexes 1 and 2 exhibit similar DPV and CV curves, and they featured higher potentials at the high oxidation state, as shown in Figures S9 and S10 in the Supporting Information and Table 2. These differences were at-

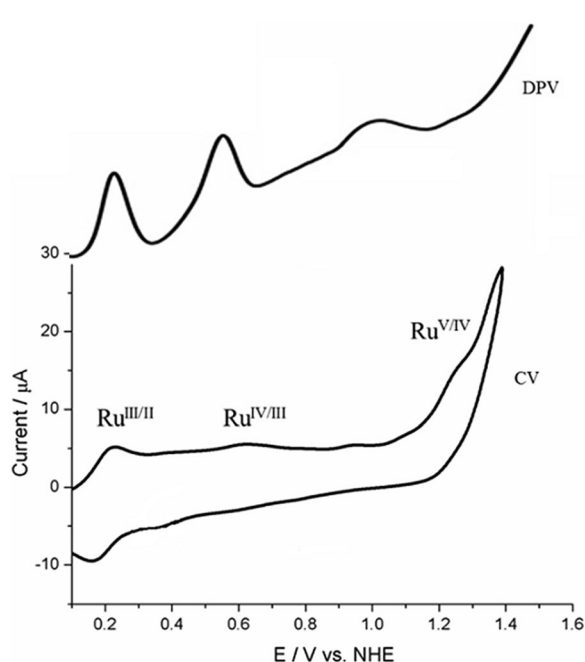


**Figure 4.** DPV and CV curves (scan rate:  $100 \text{ mV s}^{-1}$ ) of **3** in aqueous  $\text{CF}_3\text{SO}_3\text{H}$  solution (pH 1.0) containing trifluoroethanol (30%). A glassy carbon disk and Ag/AgCl were used as the working and reference electrodes, respectively.

tributed to the two substituted groups on the Schiff base ligand in the complexes. The results demonstrate that negatively charged ligands increase electron density on the  $\text{Ru}^{\text{II}}$  center, consequently lowering the oxidation potentials to gain an advantage in catalytic water oxidation.<sup>[28]</sup> The observed catalytic onsets of **1–3** are comparable with their fast current increases at around 1.30 V. The linear potential sweep voltammograms of complexes **1–3** in the mixed trifluoroethanol and  $\text{CF}_3\text{SO}_3\text{H}$  (1:2 v/v) solution were recorded and are shown in Figure S11 in the Supporting Information. It was observed that complex **3** with electron-donating methoxy groups displayed the highest current response in comparison with those of complexes **1** and **2**, which is consistent with the high catalytic efficiency of oxygen evolution. In the present system, the introduction of the phenol group has the following advantages: 1) the phenol groups in WOCs possibly form a hydrogen bond with the water molecules, which can facilitate water nucleophilic attack (WNA) reactions; and 2) the anionic group can stabilize the higher oxidation states of the  $\text{Ru}^{\text{II}}$ -based WOCs by promoting interactions between the filled p orbitals of the oxygen atom and the empty d orbital of the metal center.

To get an insight into the redox properties of these complexes, the dependence of the potentials on the pH (Pourbaix diagram) for complex **4**, which has good solubility in aqueous solution, was recorded in the pH region of 1.0 to 8.0 (Figure 5

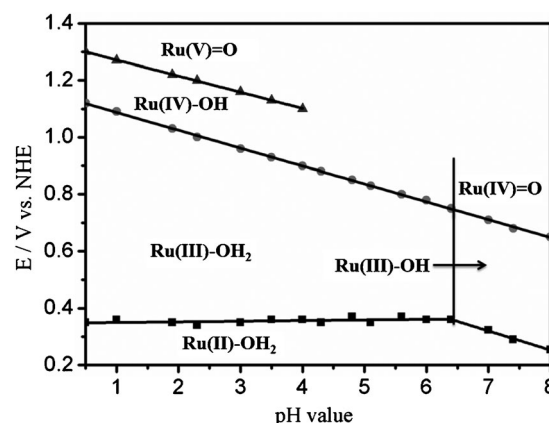


**Figure 5.** Pourbaix diagram of **4** in Britton–Robinson buffer aqueous solution. Conditions: the potentials based on the pH value were obtained from DPV measurement; the pH of the solution was adjusted by using 0.2 M NaOH aqueous solution.

and Figure S12 in the Supporting Information). Figure 5 shows the pH independence of the  $\text{Ru}^{\text{III/II}}$  process (0.35 V vs. NHE) from pH 1.0 up to 6.4 and the  $\text{p}K_{\text{a}}$  value of  $\text{Ru}^{\text{III}}\text{-OH}_2$  is 6.4. At  $\text{pH} > 6.4$  the potential for the  $\text{Ru}^{\text{III/II}}$  process follows a well-defined line with the slope close to  $-59 \text{ mV per pH unit}$ , ascribed to a  $1 \text{ e}^-/1 \text{ H}^+$  PCET process of the  $[\text{Ru}^{\text{III}}\text{-OH}]/[\text{Ru}^{\text{II}}\text{-OH}_2]$  redox couple. The  $\text{Ru}^{\text{IV/III}}$  process is pH dependent over the whole pH range from 1.0 to 8.0, with a slope of  $-59 \text{ mV per pH unit}$ , which is a typical one-electron, one-proton PCET process. The next process,  $\text{Ru}^{\text{V/IV}}$ , also has a slope of  $-59 \text{ mV per pH unit}$  from 1.0 to 4.0. Accordingly, the Pourbaix diagram of **4** supports the coordination of  $\text{H}_2\text{O}$  to the low-valent Ru center even at the  $\text{Ru}^{\text{II}}$  state and catalytic water oxidation of **4** in low pH value aqueous solution follows the redox processes from  $\text{Ru}^{\text{II}}\text{-OH}_2$  to  $\text{Ru}^{\text{III}}\text{-OH}_2$  and to  $\text{Ru}^{\text{IV}}\text{-OH}$  then to  $\text{Ru}^{\text{V}}\text{=O}$ .

### Chemical water oxidation

Chemical water oxidation was performed using CAN as the oxidant in an acidic solution. Typically, rapid oxygen evolution, as monitored by a photosensitive Ocean Optics probe, was observed upon addition of an acetonitrile solution of **1**, **2**, or **3** ( $4 \mu\text{L}$ , 1.0 mM) to  $\text{CF}_3\text{SO}_3\text{H}$  solution (4 mL, pH 1.0) containing CAN (20 mM) under vigorous stirring. The addition of acetonitrile increased the solubility of the catalyst in aqueous solution. The amount of evolved oxygen in the headspace of the reaction tube was quantified by gas chromatography (GC). Figure 6 depicts oxygen evolution curves as a function of reaction time. Oxygen production measurements were performed twice under the same conditions for the purpose of excluding the error. After 10 h, the oxygen evolution approached a plateau, generating turnover numbers (TONs) of 2400 and 3200 for **2** and **3**, respectively, whereas complex **1** produced a smaller TON of 2200. Interestingly, these complexes were remarkably stable, and oxygen evolution proceeded for over 10 h. To our knowledge, mononuclear  $\text{Ru}^{\text{II}}$ -based WOCs exhibiting good durability are scarce. The control experiments showed that in the absence of catalysts and under the same other conditions, no

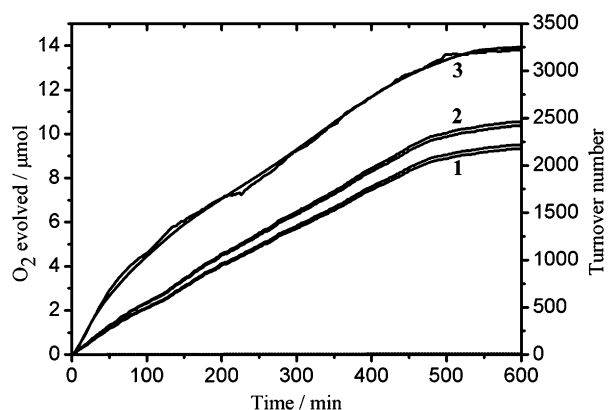


**Figure 6.** Oxygen evolution as a function of reaction time in the presence of **1** (1.0  $\mu\text{M}$ ), **2** (1.0  $\mu\text{M}$ ), or **3** (1.0  $\mu\text{M}$ ) in an aqueous  $\text{CF}_3\text{SO}_3\text{H}$  solution (pH 1.0, 4 mL) containing CAN (20 mM).

oxygen evolution was detected. Previous studies performed under strong oxidizing conditions reveal that  $\text{RuO}_2$ , which is catalytically active towards water oxidation processes, is possibly involved in the catalytic reaction.<sup>[29,30]</sup> Thus, the possible in situ formation of  $\text{RuO}_2$  nanoparticles (Figure S13 in the Supporting Information) was assessed by dynamic light scattering (DLS) experiment. The analysis confirmed that nanosized particles were not produced during the catalytic reaction. The sustained activity of the herein prepared catalysts can be explained as such: 1) the rigid Schiff base ligands are beneficial towards the robustness of the WOCs; and 2) phenolate is a hard ligand that strongly chelates to the high-valent ruthenium center.

### Mechanistic interpretation

The reaction and decay kinetic profiles were investigated by measuring the absorption decay of CAN at 360 nm after mixing the WOC with different concentrations of CAN in aqueous  $\text{HNO}_3$  solution (0.1 M, pH 1.0) through real-time UV/Vis spectroscopy. A linear dependency between the CAN depletion and the concentration of **3** was observed; the initial rate of CAN consumption was measured as  $0.65 \text{ s}^{-1}$  (Figure 7). This result indicates that complex **3** probably catalyzes water oxidation through a water nucleophilic attack mechanism proposed by Meyer et al.<sup>[31]</sup> Figure 8 shows the initial rates of oxygen evolution catalyzed by **3** as a function of catalyst concentration; the obtained profile is characteristic of a first-order reaction with a first-order rate constant of  $0.185 \text{ s}^{-1}$ . Compared with that of **3**, complexes **1** and **2** produced lower turnover frequencies of 0.097 and  $0.128 \text{ s}^{-1}$ , respectively (Figures S14–S17 in the Supporting Information). Moreover, the kinetic measurements analysis suggests that molecularly dissolved catalysts rather than  $\text{RuO}_2$  participate in the catalytic reaction. This indicates that the presence of the two methoxyl groups in **3** accelerates oxygen–oxygen bond formation. A previous study demonstrated that oxygenated groups in the vicinity of the WOC active sites are promising electron or proton donors

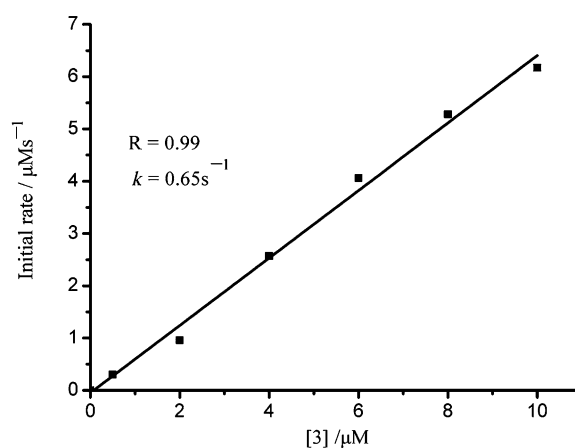
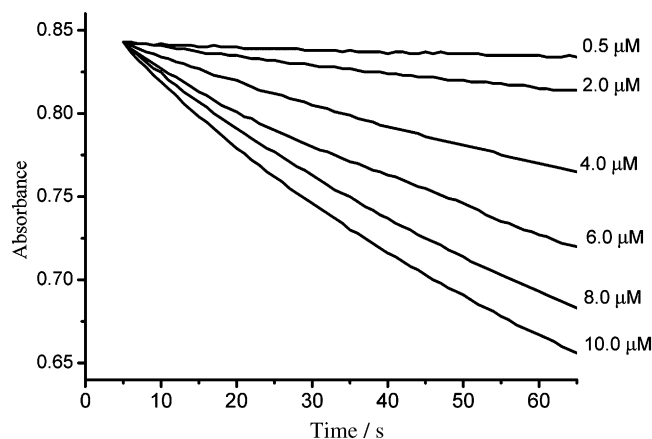


**Figure 7.** (top) Absorption spectral changes of  $(\text{NH}_4)_2\text{Ce}(\text{NO}_3)_6$  monitored at 360 nm at varying concentrations of **3** in an aqueous  $\text{HNO}_3$  solution (0.1 M, pH 1.0). Data were collected about 5 s after catalyst injection. (bottom) Initial rates of  $(\text{NH}_4)_2\text{Ce}(\text{NO}_3)_6$  consumption as a function of concentration of **3**.

and/or hydrogen-bond acceptors that are beneficial towards efficient water oxidation processes.<sup>[32]</sup>

Generally, high-valent  $\text{Ru}^{\text{V}}$ -oxo species are considered as the key active intermediate in the water oxidation by Ru-based WOCs.<sup>[33]</sup> Meyer et al. confirmed the existence of intermediate  $\text{L}_5\text{Ru}^{\text{V}}=\text{O}$  (in which  $\text{L}_5$  denotes a polypyridylic ligand) in catalyzed water oxidation processes by spectroscopic study and density functional theory calculation. Also, the nucleophilic attack of a water molecule on  $\text{Ru}^{\text{V}}=\text{O}$ , which generated three peroxidic intermediates, was reported.<sup>[34]</sup> In addition, a seven-coordinated  $\text{Ru}^{\text{V}}=\text{O}$  species is favored for Ru–bda WOCs.<sup>[35]</sup> The detection and characterization of stable intermediates during the catalytic cycle are of fundamental importance to study catalytic reaction mechanisms. To this effect, HRMS was used to probe active intermediates under the present catalytic conditions. In a typical run, CAN (10 equiv) was added to an aqueous solution of **2** (pH 1.0) under vigorous stirring and the solution was immediately injected into the mass spectrometer without any treatment. The resulting mass spectra are shown in Figure 9 and Figures S18 and S19 in the Supporting Information. A signal at  $m/z=674.1213$  was observed in the positive mode that was assigned to  $[(\text{L}2)\text{Ru}^{\text{III}}(\text{isoq})_2]^+$  species. The weak signal at  $m/z=690.1073$  was attributed to intermediate  $[(\text{L}2)-$

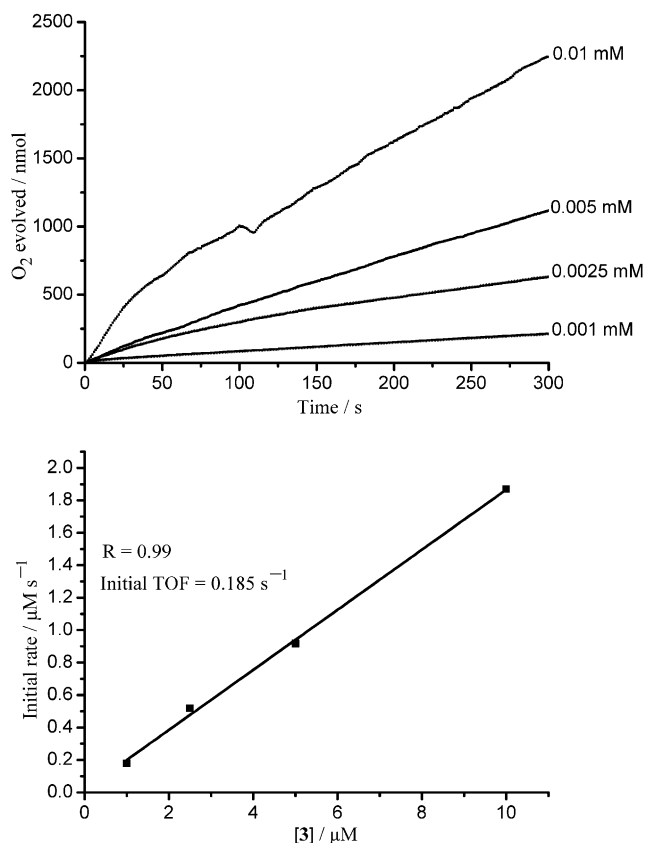


**Figure 8.** (top) Oxygen evolution profiles over 5 min at various concentrations of **3** in an aqueous  $\text{CF}_3\text{SO}_3\text{H}$  solution (pH 1.0, 4 mL) containing CAN (20 mM) at room temperature. (bottom) Initial rate of  $\text{O}_2$  production at various concentrations of **3**. The data were measured using an oxygen probe (YSI 5331) immersed in the reaction solution.

$(\text{isoq})_2\text{Ru}^{\text{V}}=\text{O}]^+$  (calculated: 690.1210), but we did not observe the signals of  $[(\text{L}2)\text{Ru}^{\text{II}}(\text{isoq})(\text{H}_2\text{O}) + \text{H}]^+$  or  $[(\text{L}2)\text{Ru}^{\text{II}}(\text{H}_2\text{O})_2 + \text{H}]^+$ . However, under acidic conditions (pH 1.0), one phenolate ligation in the complex is possibly labile and substitution by water would generate a six-coordinated aqua ruthenium complex  $\text{Ru}^{\text{II}}-\text{OH}_2$ . The dissociated phenolate moiety would then coordinate to the high-valent metal center to form a seven-coordinate species during the catalytic reaction, as evidenced by HRMS measurements. Relevant work is in progress in our laboratory. A series of high-valent intermediates is sequentially generated through PCET processes to form  $\text{Ru}^{\text{V}}=\text{O}$  species, which then undergo O–O coupling with water to generate  $\text{Ru}^{\text{III}}-\text{O}-\text{OH}$ . The latter is rapidly oxidized to  $\text{Ru}^{\text{IV}}-\text{O}-\text{O}$ , which produces oxygen through a reductive elimination step to regenerate the  $\text{Ru}^{\text{II}}-\text{OH}_2$  species (Scheme 2).

## Conclusion

Four mononuclear ruthenium(II) complexes containing different Schiff base and axial ligands were successfully synthesized. The complexes show remarkable catalytic activities and high stabilities towards CAN-driven water oxidation, and a high TON of 3200 was achieved. Kinetics studies revealed a first-order reaction process. The active intermediate  $[(\text{L})(\text{isoq})_2\text{Ru}^{\text{V}}=\text{O}]^+$  in-

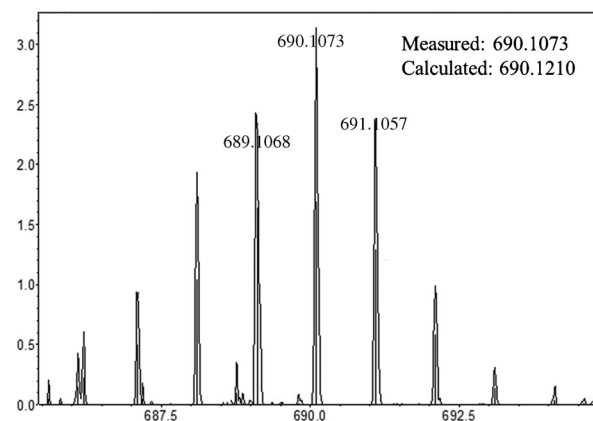
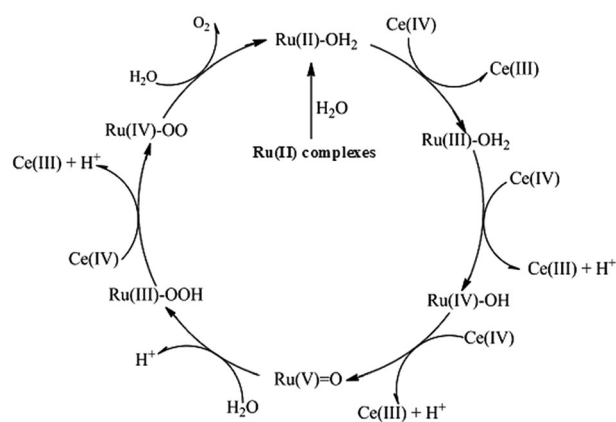


**Figure 9.** HRMS spectrum of  $[(\text{L}2(\text{isoq})_2\text{Ru}^{\text{V}}=\text{O})]^+$ : measured isotopic distribution.



**Scheme 2.** Proposed mechanism for water oxidation catalyzed by WOCs.

involved in the catalyzed water oxidation process was successfully characterized by high-resolution mass spectrometry. The introduction of electron-donating methoxyl groups of the dianionic Schiff base ligands accelerated the WNA process, which resulted in increased water oxidation rates. Studies to integrate these catalysts in a photocatalytic water redox system to investigate the structure–activity relationship are currently under way.

## Experimental Section

### General

$[\text{Ru}(\text{dmsO})_4\text{Cl}_2]^{[36]}$  and  $[\text{Ru}(\text{bpy})_3\text{Cl}_2]^{[37]}$  were prepared according to the respective reported procedures. All of the commercially available reagents and solvents used in this study were analytically pure and used without further purification. The solvents used for UV/Vis measurements were of HPLC grade.  $^1\text{H}$  NMR spectra were recorded on a Bruker Avance 400 spectrometer with chemical shifts ( $\delta$ , ppm) relative to tetramethylsilane. The mass spectra were determined on an APEX II Model FT ion cyclotron resonance mass spectrometer. Matrix-assisted laser desorption/ionization time-of-flight (MALDI-TOF) mass spectra were recorded on a Bruker BIFLEX III mass spectrometer. Elemental analyses were performed on

a Vario EL III instrument. UV/vis absorption spectra were obtained on a Hitachi U-3010 spectrophotometer. Single crystals of **2** were obtained by slow diffusion of diethyl ether vapors into an acetonitrile solution. The diffraction data were collected on a Rigaku RAXIS RAPID IP X-ray diffractometer using a graphite monochromator with  $\text{MoK}\alpha$  radiation ( $\lambda = 0.071073$  nm) at 113 K. The molecular structure of the prepared complexes was resolved by direct methods and refined by full-matrix least-squares methods on all  $F^2$  data (SHELXL-97). Non-hydrogen atoms were refined anisotropically. The position of the hydrogen atoms was calculated and refined isotropically.

### Electrochemistry

Electrochemical measurements were carried out on a CHI660C electrochemical potentiostat. Cyclic voltammetry (CV) and differential pulse voltammetry (DPV) were performed using a three-electrode cell in aqueous  $\text{CF}_3\text{SO}_3\text{H}$  solution (pH 1.0) containing trifluoroethanol (30%). Tetrabutylammonium hexafluorophosphate ( $(\text{Bu})_4\text{NPF}_6$ , 0.1 M) in acetonitrile was used as the supporting electrolyte. A glassy carbon disk (diameter: 3 mm), a platinum plate, and an Ag/AgCl electrode (3 M KCl aqueous solution) were used as the working, counter, and reference electrodes, respectively. The working electrode was successively polished with 3 and 1 mm diamond pastes and sonicated in ion-free water before use. The electrolyte was degassed with nitrogen for 30 min. All potentials are reported versus NHE, and the redox couple  $[\text{Ru}(\text{bpy})_3]^{3+}/[\text{Ru}(\text{bpy})_3]^{2+}$ ,  $E_{1/2} = 1.26$  V versus NHE, was used as a standard; the scan rate was  $100 \text{ mVs}^{-1}$ .

### Oxygen evolution analysis

An oxygen probe (YSI 5331), monitor (YSI 5300), gas chromatograph, and an Ocean Optics optical probe were used to measure and calibrate the evolved oxygen.

### Turnover frequency and kinetics of oxygen evolution

The catalytic reaction was performed in a 16 mL Schlenk bottle containing degassed aqueous  $\text{CF}_3\text{SO}_3\text{H}$  solution (pH 1.0, 4 mL) and  $\text{Ce}(\text{NH}_4)_2(\text{NO}_3)_6$  (20 mM) in an argon atmosphere. The initial rate of oxygen evolution over the course of 5 min was measured using an oxygen probe immersed in the reaction solutions. The degassed acetonitrile solution (10–100  $\mu\text{L}$ ) of **1** (1 mM) or **2** (1 mM) was introduced at the bottom of the bottle by using a microsyringe. Turnover frequency =  $(n_{\text{oxygen}}/n_{\text{catalyst}})/\text{time}$ .

### Turnover number

In a typical measurement, an aqueous solution (4 mL, 20 mM, pH 1.0 adjusted with  $\text{CF}_3\text{SO}_3\text{H}$ ) of CAN was introduced into a 25 mL reaction flask. The reaction mixture was stirred magnetically, degassed with argon for more than 30 min, and the flask was sealed with a rubber stopper. The catalyst solution (4  $\mu\text{L}$ , 1 mM) was then added to the above solution. The evolved oxygen in the headspace of the flask was monitored with a photosensitive Ocean Optics probe that was introduced into the neck of the flask. When evolution of oxygen was complete, an aliquot of the evolved gas was sampled from the headspace of the flask by using a microsyringe, and quantified by GC on a Shimadzu GC-2014 instrument equipped with a 5 Å molecular sieve column (3 m  $\times$  2 mm), a thermal conductivity detector, and argon as carrier gas. The TONs were calculated based on the catalysts.

### Dynamic light scattering analysis

DLS measurements were carried out on a Dybapro Nano Star (Wyatt Technology) instrument. The experiments were performed in an acidic solution (pH 1.0) that contained the catalyst (1.0  $\mu\text{M}$ ) and CAN (20 mM).

### Detection of intermediates by HRMS

A solution of catalyst **2** (0.05 mM, 5 mL) in acetonitrile/water (1:9) was introduced into a 20 mL flask and stirred vigorously using a magnetic bar. Then, CAN (2.5  $\mu\text{mol}$ , 10 equiv based on **2**) in aqueous  $\text{CF}_3\text{SO}_3\text{H}$  solution (100  $\mu\text{L}$ , pH 1.0) was slowly introduced. After addition of CAN, the reaction solution was immediately injected into the mass spectrometer without any treatment.

### Synthesis of complexes 1–3

A mixture of ligand  $\text{H}_2\text{L}_1$  (113 mg, 0.32 mmol),  $\text{H}_2\text{L}_2$  (100 mg, 0.32 mmol), or  $\text{H}_2\text{L}_3$  (119 mg, 0.32 mmol) and potassium acetate (63 mg, 0.64 mmol) was dissolved in *N,N*-dimethylformamide (10 mL) under a  $\text{N}_2$  atmosphere. The resulting solution was stirred vigorously and heated at  $70^\circ\text{C}$  until a color change from orange to red was observed.  $[\text{Ru}(\text{dmsO})_4\text{Cl}_2]$  (153 mg, 0.32 mmol) was then added to this solution over the course of 30 min and the mixture was warmed for 24 h. Then, excess isoquinoline (2 mL) was added to the reaction mixture, which was stirred overnight. The solvent was removed in vacuo and the resulting residue was purified by column chromatography (1:1 (v/v) hexane/dichloromethane eluent) to afford dark red solid **1–3**.

**Complex 1:** Yield: 46.3%.  $^1\text{H}$  NMR (400 MHz,  $[\text{D}_6]\text{DMSO}$ ):  $\delta = 9.42$  (s, 2H), 8.82 (s, 2H), 8.45 (dd,  $J = 5.6, 3.2$  Hz, 2H), 7.76 (t,  $J = 8.0$  Hz, 4H), 7.64 (d,  $J = 6.7$  Hz, 4H), 7.55 (t,  $J = 5.6$  Hz, 4H), 7.40 (dd,  $J = 5.9, 3.0$  Hz, 2H), 7.15 (d,  $J = 8.0$  Hz, 2H), 6.93 (dd,  $J = 11.3, 7.1$  Hz, 2H), 6.85 ppm (td,  $J = 7.6, 4.5$  Hz, 2H);  $^{13}\text{C}$  NMR (101 MHz,  $\text{CDCl}_3$ ):  $\delta = 159.2, 157.3, 150.1, 147.3, 140.8, 137.9, 133.2, 130.3, 128.2, 127.0, 126.4, 126.0, 124.5, 123.8, 123.0, 121.9, 121.0, 120.1, 116.5$  ppm; MS (MALDI-TOF):  $m/z$  711.1  $[\text{M}+\text{H}]^+$ ; elemental analysis calcd (%) for  $\text{C}_{38}\text{H}_{26}\text{N}_4\text{O}_2\text{F}_2\text{Ru}$ -isoquinoline: C 67.29, H 3.97, N 8.35; found: C 67.45, H 4.07, N 8.48.

**Complex 2:** Yield: 46.4%.  $^1\text{H}$  NMR (400 MHz,  $[\text{D}_6]\text{DMSO}$ ):  $\delta = 9.32$  (s, 2H), 8.43 (dd,  $J = 6.2, 3.1$  Hz, 2H), 8.13 (d,  $J = 8.2$  Hz, 2H), 7.83 (d,  $J = 5.7$  Hz, 2H), 7.78 (t,  $J = 7.1$  Hz, 2H), 7.75 (m, 4H), 7.70 (t,  $J = 8.0$  Hz, 2H), 7.62 (t,  $J = 6.9$  Hz, 2H), 7.55 (t,  $J = 6.6$  Hz, 4H), 7.35 (dd,  $J = 6.2, 3.1$  Hz, 2H), 7.32 (d,  $J = 8.0$  Hz, 2H), 6.19 ppm (br, 2H);  $^{13}\text{C}$  NMR (101 MHz,  $\text{CDCl}_3$ ):  $\delta = 153.4, 146.5, 143.9, 136.6, 136.4, 131.7, 131.2, 129.5, 128.7, 128.4, 128.0, 127.3, 127.2, 127.1, 126.1, 125.9, 121.3, 119.4, 114.2$  ppm; MS (MALDI-TOF):  $m/z$  675.1  $[\text{M}+\text{H}]^+$ ; elemental analysis calcd (%) for  $\text{C}_{38}\text{H}_{28}\text{N}_4\text{O}_2\text{Ru}$ -isoquinoline: C 70.31, H 4.39, N 8.72; found: C 70.59, H 4.70, N 8.48.

**Complex 3:** Yield: 49.0%.  $^1\text{H}$  NMR (400 MHz,  $\text{CD}_3\text{CN}$ ):  $\delta = 9.20$  (s, 2H), 8.52 (s, 2H), 8.10 (dd,  $J = 6.1, 3.3$  Hz, 2H), 7.60 (m, 4H), 7.53 (t,  $J = 5.6, 3.8$  Hz, 2H), 7.43 (m, 4H), 7.25 (d,  $J = 6.1$  Hz, 2H), 7.20 (dd,  $J = 6.1, 3.3$  Hz, 2H), 6.92 (d,  $J = 7.6$  Hz, 2H), 6.68 (d,  $J = 7.1$  Hz, 2H), 5.87 (br, 2H), 3.79 ppm (s, 6H);  $^{13}\text{C}$  NMR (101 MHz,  $\text{CDCl}_3$ ):  $\delta = 157.1, 154.4, 146.1, 143.4, 135.8, 134.9, 131.7, 131.3, 128.7, 127.7, 127.3, 127.2, 126.5, 126.0, 125.2, 121.8, 121.2, 120.1, 113.5, 55.9$  ppm; MS (MALDI-TOF):  $m/z$  735.1  $[\text{M}+\text{H}]^+$ ; elemental analysis calcd (%) for  $\text{C}_{40}\text{H}_{32}\text{N}_4\text{O}_4\text{Ru}$ -dmsO: C 62.13, H 4.72, N 6.90; found: C 61.86, H 4.78, N 6.98.

**Complex 4:** Yield: 45.7%.  $^1\text{H}$  NMR (400 MHz,  $[\text{D}_6]\text{DMSO}$ ):  $\delta = 9.35$  (s, 2H), 8.33 (d,  $J = 5.6$  Hz, 2H), 7.68 (d,  $J = 6.3$  Hz, 4H), 7.27 (dd,  $J = 6.2, 3.3$  Hz, 2H), 7.17 (d,  $J = 8.0$  Hz, 2H), 6.96 (d,  $J = 5.8$  Hz, 4H), 6.93

(d,  $J=7.4$  Hz, 2H), 6.20 (td,  $J=12.3$ , 4.6 Hz, 2H), 2.12 ppm (s, 6H); MS (MALDI-TOF):  $m/z$  639.1 [ $M+H$ ]<sup>+</sup>; elemental analysis calcd (%) for C<sub>32</sub>H<sub>27</sub>N<sub>4</sub>O<sub>2</sub>F<sub>2</sub>Ru: C 60.18, H 4.26, N 8.77; found: C 60.25, H 4.33, N 8.61.

CCDC-934249 and 986430 contain the supplementary crystallographic data for this paper. These data can be obtained free of charge from The Cambridge Crystallographic Data Centre via [www.ccdc.cam.ac.uk/data\\_request/cif](http://www.ccdc.cam.ac.uk/data_request/cif).

## Acknowledgements

This work was supported by the National Key Basic Research Program of China (973 Program 2013CB834804 and 2013CB632403) and by the Ministry of Science and Technology of China (2012DFH40090). We thank the Natural Science Foundation of China (NSFC Grant Nos. 21267025, 21273257, and U1137606), CAS-Croucher Funding Scheme for Joint Laboratories, and Yunnan Key Project (2010CC007) for financial support. Y.C. acknowledges the Chinese Academy of Sciences (100 Talents Program) for funding support.

**Keywords:** homogeneous catalysis · ruthenium · Schiff bases · water oxidation · water splitting

- [1] E. Amouyal, *Sol. Energy Mater. Sol. Cells* **1995**, *38*, 249–276.  
 [2] N. S. Lewis, D. G. Nocera, *Proc. Natl. Acad. Sci. USA* **2006**, *103*, 15729–15735.  
 [3] D. G. Nocera, *ChemSusChem* **2009**, *2*, 387–390.  
 [4] J. L. Dempsey, A. J. Esswein, D. R. Manke, J. Rosenthal, J. D. Soper, D. G. Nocera, *Inorg. Chem.* **2005**, *44*, 6879–6892.  
 [5] K. N. Ferreira, T. M. Iverson, K. Maghlaoui, J. Barber, S. Iwata, *Science* **2004**, *303*, 1831–1838.  
 [6] N. Kamiya, J.-R. Shen, *Proc. Natl. Acad. Sci. USA* **2003**, *100*, 98–103.  
 [7] B. Loll, J. Kern, W. Saenger, A. Zouni, J. Biesiadka, *Nature* **2005**, *438*, 1040–1044.  
 [8] A. Zouni, H.-T. Witt, J. Kern, P. Fromme, N. Krauss, W. Saenger, P. Orth, *Nature* **2001**, *409*, 739–743.  
 [9] G. C. Dismukes, R. Brimblecombe, G. A. Felton, R. S. Pryadun, J. E. Sheats, L. Spiccia, G. F. Swiegers, *Acc. Chem. Res.* **2009**, *42*, 1935–1943.  
 [10] a) J. J. Concepcion, J. W. Jurss, M. K. Brennaman, P. G. Hoertz, A. O. T. Patrocínio, N. Y. M. Iha, J. L. Templeton, T. J. Meyer, *Acc. Chem. Res.* **2009**, *42*, 1954–1965; b) X. Liu, F. Wang, *Coord. Chem. Rev.* **2012**, *256*, 1115–1136; c) L. Bernet, R. Lalrempuia, W. Ghattas, H. Müller-Bunz, L. Vigarà, A. Llobet, M. Albrecht, *Chem. Commun.* **2011**, *47*, 8058–8060; d) M. Ven-nampalli, G. Liang, C. E. Webster, X. Zhao, *Eur. J. Inorg. Chem.* **2014**, *4*, 715–721.  
 [11] a) N. D. McDaniel, F. J. Coughlin, L. L. Tinker, S. Bernhard, *J. Am. Chem. Soc.* **2008**, *130*, 210–217; b) J. F. Hull, D. Balcells, J. D. Blakemore, C. D. Incarvito, O. Eisenstein, G. W. Brudvig, R. H. Crabtree, *J. Am. Chem. Soc.* **2009**, *131*, 8730–8731; c) R. Lalrempuia, N. D. McDaniel, H. Müller-Bunz, S. Bernhard, M. Albrecht, *Angew. Chem.* **2010**, *122*, 9959–9962; *Angew. Chem. Int. Ed.* **2010**, *49*, 9765–9768.  
 [12] a) F. M. Ashmawy, C. A. McAuliffe, R. D. Parish, J. Tames, *J. Chem. Soc. Dalton Trans.* **1985**, *7*, 1391–1397; b) J. Limburg, J. S. Vrettos, L. M. Liable-Sands, A. L. Rheingold, R. H. Crabtree, G. W. Brudvig, *Science* **1999**, *283*, 1524–1527; c) E. A. Karlsson, B.-L. Lee, T. Åkermark, E. V. Johnston, M. D. Kärkäs, J. Sun, Ö. Hansson, J.-E. Bäckvall, B. Åkermark, *Angew. Chem.* **2011**, *123*, 11919–11922; *Angew. Chem. Int. Ed.* **2011**, *50*, 11715–11718.  
 [13] a) W. C. Ellis, N. D. McDaniel, S. Bernhard, T. J. Collins, *J. Am. Chem. Soc.* **2010**, *132*, 10990–10991; b) J. L. Fillol, Z. Codolà, I. Garcia-Bosch, L. Gómez, J. J. Pla, M. Costas, *Nat. Chem.* **2011**, *3*, 807–813; c) D. Hong, S. Mandal, Y. Yamada, Y. M. Lee, W. Nam, A. Llobet, S. Fukuzumi, *Inorg. Chem.* **2013**, *52*, 9522–9531.  
 [14] a) D. J. Wasylenko, C. Ganesamoorthy, J. Borau-Garcia, C. P. Berlinguette, *Chem. Commun.* **2011**, *47*, 4249–4251; b) S. Berardi, G. La Ganga, M. Natali, I. Bazzan, F. Puntoriero, A. Sartorel, F. Scandola, S. Campagna, M. Bonchio, *J. Am. Chem. Soc.* **2012**, *134*, 11104–11107; c) T. Nakazono, A. R. Parent, K. Sakai, *Chem. Commun.* **2013**, *49*, 6325–6327.  
 [15] S. W. Gersten, G. J. Samuels, T. J. Meyer, *J. Am. Chem. Soc.* **1982**, *104*, 4029–4030.  
 [16] R. F. Zong, R. P. Thummel, *J. Am. Chem. Soc.* **2005**, *127*, 12802–12803.  
 [17] a) L. Duan, A. Fischer, Y. Xu, L. Sun, *J. Am. Chem. Soc.* **2009**, *131*, 10397–10399; b) L. Duan, Y. Xu, P. Zhang, M. Wang, L. Sun, *Inorg. Chem.* **2009**, *48*, 209–215.  
 [18] L. Duan, F. Bozoglian, S. Mandal, B. Stewart, T. Privalov, A. Llobet, L. Sun, *Nat. Chem.* **2012**, *4*, 418–423.  
 [19] D. J. Wasylenko, C. Ganesamoorthy, B. D. Koivisto, M. A. Henderson, C. P. Berlinguette, *Inorg. Chem.* **2010**, *49*, 2202–2209.  
 [20] a) Z. Chen, J. J. Concepcion, J. W. Jurss, T. J. Meyer, *J. Am. Chem. Soc.* **2009**, *131*, 15580–15581; b) J. Mola, E. Mas-Marza, X. Sala, I. Romero, M. Rodríguez, C. Vinas, T. Parella, A. Llobet, *Angew. Chem.* **2008**, *120*, 5914–5916; *Angew. Chem. Int. Ed.* **2008**, *47*, 5830–5832; c) F. Li, B. Zhang, X. Li, Y. Jiang, L. Chen, Y. Li, L. Sun, *Angew. Chem.* **2011**, *123*, 12484–12487; *Angew. Chem.* **2011**, *123*, 12484–12487.  
 [21] L. Tong, L. Duan, Y. Xu, T. Privalov, L. Sun, *Angew. Chem.* **2011**, *123*, 465–469; *Angew. Chem. Int. Ed.* **2011**, *50*, 445–449.  
 [22] a) P. G. Cozzi, *Chem. Soc. Rev.* **2004**, *33*, 410–421; b) C. Baleizão, H. Garcia, *Chem. Rev.* **2006**, *106*, 3987–4043; c) K. C. Gupta, A. K. Sutar, *Coord. Chem. Rev.* **2008**, *252*, 1420–1450.  
 [23] M. D. Kärkäs, T. Åkermark, E. V. Johnston, S. R. Karim, T. M. Laine, B.-L. Lee, T. Åkermark, T. Privalov, B. Åkermark, *Angew. Chem.* **2012**, *124*, 11757–11761; *Angew. Chem. Int. Ed.* **2012**, *51*, 11589–11593.  
 [24] C. F. Works, C. J. Jocher, G. D. Bart, *Inorg. Chem.* **2002**, *41*, 3728–3739.  
 [25] K. Chichak, U. Jacquemard, N. R. Branda, *Eur. J. Inorg. Chem.* **2002**, *2002*, 357–368.  
 [26] N. Kaveevivitchai, R. Zong, H.-W. Tseng, R. Chitta, R. P. Thummel, *Inorg. Chem.* **2012**, *51*, 2930–2939.  
 [27] a) H. W. Tseng, R. Zong, J. T. Muckerman, R. Thummel, *Inorg. Chem.* **2008**, *47*, 11763–11773; b) Y. Xu, L. Duan, T. Åkermark, L. Tong, B. L. Lee, R. Zhang, B. Åkermark, L. Sun, *Chem. Eur. J.* **2011**, *17*, 9520–9528.  
 [28] L. Duan, Y. Xu, M. Gorlov, L. Tong, S. Andersson, L. Sun, *Chem. Eur. J.* **2010**, *16*, 4659–4668.  
 [29] K. Nagoshi, S. Yamashita, M. Yagi, M. J. Kaneko, *J. Mol. Catal. A* **1999**, *144*, 71–76.  
 [30] Y. Zhang, E. C. Judkins, D. R. McMillin, D. Mehta, T. Ren, *ACS Catal.* **2013**, *3*, 2474–2478.  
 [31] J. J. Concepcion, J. W. Jurss, J. L. Templeton, T. J. Meyer, *J. Am. Chem. Soc.* **2008**, *130*, 16462–16463.  
 [32] D. C. Marelus, S. Bhagan, D. J. Charboneau, K. M. Schroeder, J. M. Kamdar, A. R. McGettigan, B. J. Freeman, C. E. Moore, A. L. Rheingold, A. L. Cooksy, D. K. Smith, J. J. Paul, E. T. Papish, D. B. Grotjahn, *Eur. J. Inorg. Chem.* **2014**, *4*, 676–689.  
 [33] S. Romain, L. Vigarà, A. Llobet, *Acc. Chem. Res.* **2009**, *42*, 1944–1953.  
 [34] J. J. Concepcion, M. K. Tsai, J. T. Muckerman, T. J. Meyer, *J. Am. Chem. Soc.* **2010**, *132*, 1545–1557.  
 [35] L. Duan, L. Wang, A. K. Inge, A. Fischer, X. Zou, L. Sun, *Inorg. Chem.* **2013**, *52*, 7844–7852.  
 [36] E. Dulière, M. Devillers, J. Marchand-Brynaert, *Organometallics* **2003**, *22*, 804–811.  
 [37] J. A. Broomhead, C. G. Young, *Inorg. Synth.* **1982**, *21*, 127–128.

Received: December 23, 2013  
 Published online on June 2, 2014